JOURNAL OF GEOPHYSICAL RESEARCH, VOL. 94, NO. B11, PAGES 15,703–15,721, NOVEMBER 10, 1989

Particle Size Distributions and the Sequential Fragmentation/Transport Theory Applied to Volcanic Ash

K. H. WOHLETZ

Earth and Space Science Division, Los Alamos National Laboratory, New Mexico

M. F. SHERIDAN

Department of Geology, Arizona State University, Tempe

W. K. BROWN

Math/Science Division, Lassen College, Susanville, California

The assumption that distributions of mass versus size interval for fragmented materials fit the log normal distribution is empirically based and has historical roots in the late 19th century. Other often used distributions (e.g., Rosin-Rammler, Weibull) are also empirical and have the general form for mass per size interval: $n(l) = kl^{\alpha} \exp(-l^{\beta})$, where $n(l)$ represents the number of particles of diameter l, l is the normalized particle diameter, and k, α, and β are constants. We describe and extend the sequential fragmentation distribution to include transport effects upon observed volcanic ash size distributions. The sequential fragmentation/transport (SFT) distribution is also of the above mathematical form, but it has a physical basis rather than empirical. The SFT model applies to a particle-mass distribution formed by a sequence of fragmentation (comminution) and transport (size sorting) events acting upon an initial mass m': $n(x, m) = C \iint n(x', m')p(\xi)\, dx'\, dm'$, where x' denotes spatial location along a linear axis, C is a constant, and integration is performed over distance from an origin to the sample location and mass limits from 0 to m. We show that the probability function that models the production of particles of different size from an initial mass and sorts that distribution, $p(\xi)$, is related to m^g, where g (noted as γ for fragmentation processes) is a free parameter that determines the location, breadth, and skewness of the distribution; g (γ) must be greater than -1, and it increases from that value as the distribution matures with greater number of sequential steps in the fragmentation or transport process; γ is expected to be near -1 for "sudden" fragmentation mechanisms such as single-event explosions and transport mechanisms that are functionally dependent upon particle mass. This free parameter will be more positive for evolved fragmentation mechanisms such as ball milling and complex transport processes such as saltation. The SFT provides better fits to many types of volcanic ash samples than does the log normal curve. Modeling of the SFT shows its similarity to the log normal curve on size frequency histograms; it differs by its variable skewness controlled by γ. Skewed distributions are typical of many volcanic ash samples, and characterization of them by the SFT allows interpretation of eruptive and transport mechanisms.

1. INTRODUCTION

Particle size-frequency distributions have been a topic of considerable study not only in geophysical sciences but in industrial-related work for nearly a century. This topic fits into a category of general scientific studies of frequency curves, a topic of statistical analysis [*Elderton and Johnson*, 1969]. In general, the study of size distributions in geophysics has been based upon empirical mathematical characterizations of mass or diameter distributions. In scientific studies such as size distributions of stars, asteroids, and sediments, workers seek to not only characterize distributions but interpret them as well. Application of empirical distribution laws affords little fundamental physical interpretation. Our recent research on the particle-size distributions of volcanic ash has led us to develop an approach which we believe provides a direct link to underlying physical processes.

Sheridan [1971] pointed out problems in characterization and interpretation of size-frequency distributions of tephra by the lognormal distribution law. Other distributions such as the Rosin-Rammler [*Kittleman*, 1964] and the Weibull [*Nakamura*, 1984] have been proposed as alternatives in that their forms better fit the distribution of the finer particle sizes. More recently, *Sheridan et al.* [1987] discussed the polymodal nature of tephra size distributions and a method for decomposition of subpopulations prior to characterization. Still, the underlying mathematical form of size subpopulations was assumed to be log normal. This assumption of an empirical mathematical form hampers even interpretations based upon newly proposed methods utilizing fractal dimensions [*Turcotte*, 1986].

A newly developed method of understanding mass-frequency distributions, called "sequential fragmentation theory" [*Brown*, 1989] in application to processes of continuing comminution, offers perhaps the first approach that allows development of a generalized physical model. *Brown* [1986] shows how this theory works well for characterization of the initial mass function of stars, and he later [*Brown*, 1989] shows that this theory well approximates measured distributions for a number of different materials including

Paper number 89JB01248.
0148-0227/89/89JB-01248$05.00

high explosive aerosols, infalling extraterrestrial material, black magnetic spherules from deep sea sediments, the asteroids, volcanic ash and its experimental analog, and ball mill products. As a result of the success of these initial applications, we specifically develop the theory for application to geologic materials, using volcanic ash as an example.

There are several important considerations in applying our fragmentation theory to volcanic ash. Among those we consider most important are bias introduced by sampling technique, limitations of the size measurement system, and generalization of the physical processes responsible for production of volcanic ash and its transport to the sampling point. The first two considerations have been topics resolved by previous workers [*Folk*, 1974; *Krumbein*, 1938; *Wentworth*, 1922]. An implicit caveat is that samples represent a statistically significant collection of particles from a single deposit. Typically, particles sizes are measured by sieving, which introduces a shape bias, as do settling velocity techniques. Comparisons of optical measurements, utilizing scanning electron microscopy and optical microscopes, with sieve measurements show a general agreement between the two methods for most volcanic ash samples. Typically, size data are expressed by mass abundances in bins spaced by logarithmic size intervals. This method minimizes the effect of shape bias for all except particles of geologically extreme shape. The final bias, that of generalization of fragmentation physics and effect of transport on a population of particles, incorporates the basic assumption that a size distribution of volcanic ash is a unique signature of the process or processes responsible for its formation. The validity of this assumption has been demonstrated by numerous studies of field samples [*Walker*, 1971; *Sheridan*, 1971; *Sheridan and Updike*, 1975; *Carey and Sigurdsson*, 1982; *Wohletz*, 1983; *Sheridan et al.*, 1987] as well as laboratory and theoretical arguments [*Anderson and Hallet*, 1986; *Kranck and Milligan*, 1985; *Iversen and White*, 1982].

The objectives of this paper are (1) to present a brief review of mathematical representations of particle size distributions; (2) to develop the sequential fragmentation/transport (SFT) theory; (3) to demonstrate application of the model with representative sets of volcanic ash data; (4) to briefly interpret results of the SFT model. With respect to the second objective, we do not intend to develop the detailed physics, but we attempt to show how the SFT model predicts the size-frequency distribution form that should be produced by most physical processes of fragmentation and subsequent geologic transport. Readers who are primarily interested in the geologic application of the model may wish to skip the mathematical derivations that follow and begin with section 4. Throughout the manuscript, we use a common notation for which important symbols are n, which represents the number or number distribution, l, which is a particle diameter, and m, which is particle mass (see notation list after the appendix). In general, m and l are nondimensionalized by division by a standard unit of mass and length, respectively. Upper case forms of these symbols represent their cumulative value over a specified interval, and where these upper case symbols are subscripted with t the total value of the population is meant. In several places we have assumed that a spherical shape and constant density are statistically appropriate for conversion of fragment mass to a function of fragment diameter. Because this assumption is not always appropriate for geological materials, we show how the SFT model accommodates these complexities.

2. HISTORY OF SIZE DISTRIBUTIONS

Most early researchers who were investigating distributions of particles sought to characterize their data using empirical size distribution functions. These functions were useful in correlating limited data sets, but they neither revealed the physical phenomena that gave rise to the forms seen in the data, nor did they allow extrapolation beyond the range of data. Below, we summarize evolution of models regarding size distributions from early analytical forms through empirical models based upon industrial processes to the well-known lognormal distribution.

Early Analytical Forms

Many early forms were simple power laws, for example, that of *Mellor* [1910] who proposed that the particle number per size class is constant, or

$$n(l) = c_1 \tag{1}$$

where $n(l)$ is the number of particles per size class between l and $l + dl$, and c_1 is a constant. *Brown* [1989] relates the mass distribution $mn(m)$ to the particle number distribution by

$$mn(m) = \tfrac{1}{3}\, l\ n(l) \tag{2}$$

where $n(m)$ is the particle number distribution in mass and denotes the number of particles per unit mass m between m and $m + dm$. Because $l \propto m^{1/3}$ for spherical and equidimensional blocky particles, Mellor's formula can also be stated

$$mn(m) = c_2 m^{1/3} \tag{3}$$

where c_2 is a constant. Although equation (1) is based on assumption and not experiment, we will show later that it is an adequate description of the "fines" in some distributions.

Another proposal [*Vieweg*, 1935] is that

$$n(l) = c_3 l^{-4} \tag{4}$$

which translates into the mass distribution

$$mn(m) = c_4 m^{-1} \tag{5}$$

Vieweg was apparently working with a sample containing the heavier portion of a distribution, but over his range of data, equation (5) was an adequate approximation.

Martin et al. [1923] used another simple form when they proposed that

$$n(l) = c_5 e^{-bl} \tag{6}$$

Equation (6) translates into

$$mn(m) = c_6 m^{1/3} \exp\left[-m^{1/3}\right] \tag{7}$$

In fact, *Pearson* [1895] had earlier proposed two extreme cases: that of equation (6), and also that of

$$n(l) = c_7 e^{-bl^2} \tag{8}$$

or

$$mn(m) = c_8 m^{1/3} \exp\left[-m^{2/3}\right] \tag{9}$$

Between Pearson's two extremes we find that

$$mn(m) = c_9 m^{1/3} \exp[-m^{\beta}] \quad (10)$$

where $1/3 \leq \beta \leq 2/3$.

Later, *Rietz* [1922] also proposed a form similar to equation (10), built on the normal curve of error, equation (8), that entailed replacing l with l^n.

As we shall show later, although such forms as those of *Pearson* [1895] and *Martin et al.* [1923] had no basis in physical theory, they anticipated sequential fragmentation theory [*Brown*, 1989] by decades.

More Sophisticated Empirical Forms From Grinding, Milling, and Fragmentation

In the 1930s, when the world was running largely on coal-fed power, knowledge of the particle size distribution of crushed coal was important in understanding its burning characteristics. *Rosin and Rammler* [1933] and *Rosin* [1937] proposed an empirical description of powdered coal. In our present terminology their law is

$$\frac{M(>l)}{M_t} = \exp\left[-\left(\frac{l}{\sigma}\right)^k\right] \quad (11)$$

where $M(>l)$ is the cumulative mass of all particles in the distribution of size greater than l, M_t is the total mass of particles in the distribution, σ is a size related to the average particle size in the distribution, and k is a free parameter. *Rosin and Rammler* [1934] also used equation (11) to investigate the grinding of other materials. *Bennett* [1936] offered theoretical support for equation (11), and *Kittleman* [1964] and *Krumbein and Tisdel* [1940] have commented on its application for geological materials.

Brown [1989] points out that the Rosin-Rammler law is identical to the empirical *Weibull* [1951] distribution, given by

$$\frac{M(<l)}{M_t} = 1 - \exp\left[-\left(\frac{l}{\sigma}\right)^k\right] \quad (12)$$

The Weibull distribution has also been used extensively in the field of fragmentation. Recalling that $dM/dm = mn(m)$, we translate equations (11) and (12) into the mass distribution

$$mn(m) = \frac{M_t}{m_3}\frac{k}{3}\left(\frac{m}{m_3}\right)^{(k/3)-1} \exp\left[-\left(\frac{m}{m_3}\right)^{k/3}\right] \quad (13)$$

where $m/m_3 = (l/\sigma)^3$. In a wide variety of fragmentation experiments, it has been found that $1 \leq k \leq 6$ where the exponent on the fines, $\alpha = (k/3) - 1$, can vary between $-2/3 \leq \alpha \leq 1$, while the exponent in the large-mass cutoff function, $\beta = k/3$, can vary between $1/3 \leq \beta \leq 2$ (see, for example, *Brown et al.* [1983]). For coal, *Geer and Yancey* [1938] found that the "distribution factor," k, could vary over the range $0.5 < k < 1.3$, indicating that $-0.8 < \alpha < -0.6$, and that $0.17 < \beta < 0.4$.

Another empirical distribution that has been successful in the field of fragmentation is

$$\frac{N(>m)}{N_t} = \exp\left[-\left(\frac{m}{\mu}\right)^{\nu}\right] \quad (14)$$

where $N(>m)$ is the cumulative number of particles in the distribution of mass greater than m, N_t is the total number of particles in the distribution, μ is a mass related to the average mass, and ν is a free parameter. The logarithmic form of this equation has been extensively used for munitions experiments, and in cases where $\nu = 1/2$, the plot of experimental data is known as the "Mott plot." *Turcotte* [1986] cited this form in his fractal representation of fragmentation and gave an empirical power law size-frequency distribution similar to equation (4). Recalling that $n(m) = -dN/dm$, we find that

$$mn(m) = N_t \nu \left(\frac{m}{\mu}\right)^{\nu} \exp\left[-\left(\frac{m}{\mu}\right)^{\nu}\right] \quad (15)$$

Among the uses of equations (14) and (15) are characterization of fragment mass distributions from the explosions of munitions, where, typically, $\nu = 1/2$ or $1/3$.

All of the above equations (equations (1)–(15)) have the general form

$$mn(m) = c_{10}\left(\frac{m}{m_4}\right)^{\alpha} \exp\left[-\left(\frac{m}{m_4}\right)^{\beta}\right] \quad (16)$$

where $-1 \leq \alpha \leq 1$ and $0.1 \leq \beta \leq 2$. Note that α and β are linked in equations (13) and (15), although the link differs by unity.

Roller [1937, 1941] proposed the use of an empirical function with similarities to equation (16), but it is somewhat more complicated and was not extensively used.

In the history of grinding, milling, and fragmentation, equation (16) summarizes one of the two successful empirical descriptions; the second is the log normal distribution.

Log Normal Distribution

The log normal distribution was formulated on a theoretical basis by *McAlister* [1879]. As is the case of *Pearson*'s [1895] theoretical work, the applications were far in the future. For example, *Drinker* [1925] analyzed the size distribution of certain dusts by plotting $M(l)/M_t$ versus log l on probability paper (Drinker refers to "Hazen's logarithmic probability paper," but the reference is lacking). In another example, *Loveland and Trivelli* [1927*a*, *b*] used the lognormal distribution to characterize the particles in precipitates, including silver bromide precipitations in the gelatin of photographic films. In its general form, they used

$$n(l) = A_1 \exp\left[-a_1\left(\ln\left(\frac{l}{l_3}\right) - b_1\right)^2\right] \quad (17)$$

where their data generally fell on the right-hand (coarse) side of the curve. In equation (17), A_1, a_1, and b_1 are constants. Converting equation (17) to a mass distribution results in

$$mn(m) = A_2 \exp\left[-a_2\left(\ln\left(\frac{m}{m_5}\right) - b_2\right)^2\right] \quad (18)$$

The $m^{1/3}$ term arising from equation (3) has been omitted, resulting in a pure log normal distribution in mass. In any event, we note that the right-hand side of equation (18) is well approximated by the large-mass cutoff term (the exponential term) in equation (16).

Sheridan et al. [1987] characterized subpopulations of polymodal volcanic ash size distributions using

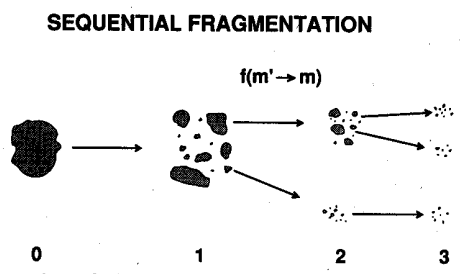

Fig. 1. Illustration of physical model for sequential fragmentation mathematically represented by equation (20) in the text. Note that each generation is an ensemble of fragments that may range in size from the very finest particles to one that is nearly as large as its parent from the previous generation. Such continued comminution produces a fragmentation cascade resembling a chain reaction.

$$m^2n(m) = A_3 \exp\left[-a_3\left(\ln\left(\frac{l}{l_4}\right) - b_2\right)^2\right] \tag{19}$$

where $m^2n(m)$ expresses the mass distribution in terms of mass per natural logarithmic interval in m in the distribution $[dM/d \ln (m) = m^2n(m)]$. Although this form proved to be an adequate model by which to characterize ash data, we will show through derivation of the sequential fragmentation/transport model that it not only better characterizes the data but also allows physical interpretation.

In general, previous workers have used the log normal distribution empirically, which allows such otherwise contradictory applications of equations (17)–(19). Although the lognormal distribution has basis in statistical theory [*McAlister*, 1879], it is not derived from a physical theory, nor is it based on a physical model.

3. Sequential Fragmentation/Transport Theory (SFT)

The present theory of sequential fragmentation/transport describes the size characteristics of a distribution of particles as they first undergo fragmentation and then attrition and size sorting during transport within a liquid or gaseous media. Because SFT is an outgrowth of sequential fragmentation theory [*Brown*, 1989], we recapitulate the fragmentation model before presenting the transport aspect of SFT.

Sequential Fragmentation

Brown [1986] sets forth the following equation to describe the sequential fragmentation process, which is an expression for conservation of mass:

$$n(m) = C_1 \int_m^\infty n(m')f(m' \rightarrow m)\, dm' \tag{20}$$

where the function $f(m' \rightarrow m)$ describes the single-event mass distribution resulting from the fragmentation of a particle of mass m' $(>m)$. C_1 is a constant. Equation (20) represents a summing of contributions from fragmenting particles of mass m' to the population of mass m below, shown schematically in Figure 1. Because mass is conserved, no assumptions concerning particle shape and density are required. One can picture a fragment of mass m' breaking up into an ensemble of smaller particles of various masses whose sum equals m'; then in succession each of the smaller particles breaking again forming numerous new ensembles. Integrated over many steps of dm', the process is a cascading mechanism analogous to a chain reaction.

For $f(m' \rightarrow m)$, *Brown* [1988] chose

$$f(m' \rightarrow m) = \left(\frac{m}{m_1}\right)^\gamma \tag{21}$$

where m_1 is a mass related to the average mass and γ is a free parameter and $\gamma \geq -1$. While equation (21) is not specific in the manner by which fragmentation occurs, *Brown* [1989] supports the choice of equation (21) with experimental data. Inserting equation (21) into equation (20) and normalizing by $C_1 = 1/m_1$,

$$n(m) = \left(\frac{m}{m_1}\right)^\gamma \int_{m/m_1}^\infty n(m')\, d(m'/m_1) \tag{22}$$

where $(m/m_1)^\gamma$ has been removed from the integral because it is a function of m, not m'. *Brown* [1989] finds the solution of equation (22) to be

$$n(m) = \frac{N_t}{m_1}\left(\frac{m}{m_1}\right)^\gamma \exp\left[-\frac{(m/m_1)^{\gamma+1}}{\gamma+1}\right] \tag{23}$$

where the distribution has been normalized so that

$$N_t = \int_0^\infty n(m)\, dm \tag{24}$$

The mass distribution per logarithmic mass interval is given by

$$m^2n(m) = N_t m_1\left(\frac{m}{m_1}\right)^{\gamma+2} \exp\left[-\frac{(m/m_1)^{\gamma+1}}{\gamma+1}\right] \tag{25}$$

It is interesting to note that *Theimer* [1952], in an attempt to derive the Rosin-Rammler equation, studied the statistical mechanics of grinding processes and produced an equation similar to equation (23). *Brown* [1989] pointed out that equation (25) is identical to equations (15) and (16), both of which have successfully characterized data from hundreds of experiments pertaining to various fragmentation mechanisms. *Brown* [1989] further validated equation (25) by successfully applying it to the data from several additional experiments including the explosive aerosolization of plutonium, the grinding of iron in a ball mill, and the production of ash by simulated volcanic explosions. Finally, *Brown* [1989] applies the sequential fragmentation theory to several astronomical phenomena that are candidates for having undergone the sequential fragmentation process; these phenomena include infalling extraterrestrial material, siderophile element concentrations in black magnetic spherules of possible meteoritic origin, the asteroids, the distribution of galactic masses, and the initial mass function of stars. Because the free parameter γ differs for different fragmentation mechanisms and it is explicitly related to mass, γ should be theoretically predictable for given physical mechanisms of fragmentation.

Sequential Transport

Because particle attrition, occurring during transport, is covered by the fragmentation theory, the transport theory includes the size distribution modification (sorting) caused by the transport mechanism, which can be safely assumed to be mass sensitive. Figure 2 shows a schematic drawing of the

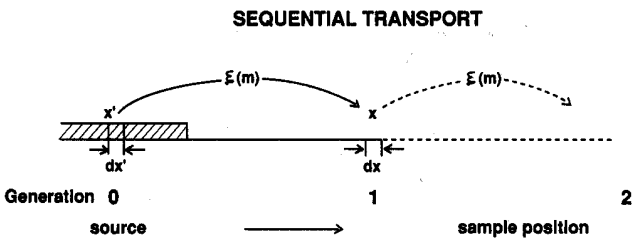

Fig. 2. Illustration of physical model for sequential transport mathematically represented by equation (36) in the text. Note that each successive generation found at location x has as its parent the ensemble of particles existing previously (and possibly transiently) at location x', which in turn might be a daughter ensemble from some previous source location.

coordinate system adapted for the basis of the present transport theory. Shown at the left of Figure 2 is the pristine pile of material from which the carrier transports particles to the right. We offer the following equation to describe the transport process, which explicitly conserves mass and implicitly conserves momentum.

$$n(x, m) = C_2 \int_0^m \int_{x-\xi}^0 n(x', m')p(\xi)\, dx'\, dm' \quad (26)$$

Here $n(x, m)$ is the particle number distribution in terms of the number of particles in the length interval between x and $x + dx$ and mass interval between m and $m + dm$. The function $p(\xi)$ is the probability that a particle carried from location x' will be deposited at location x downstream. In this way, ξ is the possible range of a particle lifted from the pile by the carrier. Equation (26) represents a summing of all particles from the original pile contributing to the population at x. This equation is exactly parallel to the sequential fragmentation equation (20), although it is complicated by the presence of two variables rather than one.

The probability, $p(\xi)$, that a particle arrives at location x is given by

$$p(\xi)\, dx = \frac{dx}{\xi} \quad (27)$$

Because $p(\xi)$ gives a distribution of particles arriving at x, it may be removed from the inner integral in equation (26), giving

$$n(x, m) = C_2 \int_0^m \xi^{-1} \int_{x-\xi}^0 n(x', m')\, dx'\, dm' \quad (28)$$

We set the range, ξ, to be generally related to the particle mass m by

$$\xi = \xi_0 \left(\frac{m}{m_2}\right)^{-g} \quad (29)$$

where g (analogous to γ in the fragmentation theory) is a free parameter, m_2 is a mass related to the average mass, and ξ_o is a length that is a function of the carrier flux, $\rho\nu$, but not the particle mass; ρ and ν are the carrier bulk density and velocity, respectively. Several dependencies are hypothetically summarized by equation (29), including the tendency of the particle to fall back to the surface, the area that it presents to the carrier fluid, and possibly its rolling and bouncing ability. For each type of transport, the physical description can be shown to be mass sensitive, thus supporting equation (29).

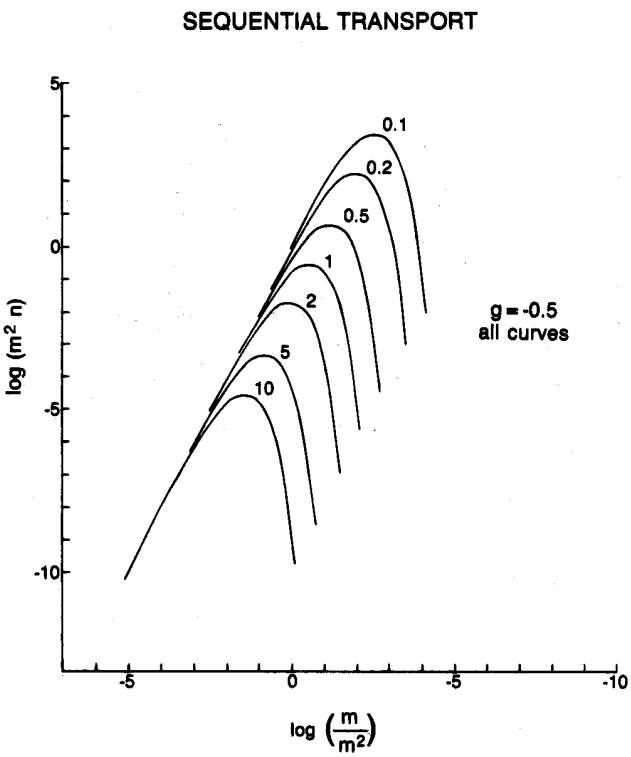

Fig. 3. Plot of the logarithm of total mass of fragments ($\log m^2 n$) versus logarithmic interval in normalized mass ($\log m/m_2$). These curves, representing equation (32) in the text, show that for increasing transport distance (x/ξ_o = 0.1, 0.2, 0.5, 1, 2, 5, 10), the shape of the distribution does not change for a given transport of constant value of g (see Appendix B).

Substituting equation (29) into equation (28) and normalizing by $C_2 = 1/m_2$,

$$n(x, m) = \int_0^{m/m_2} \left(\frac{m'}{m_2}\right)^g \int_{(x-\xi)/\xi_0}^0 n(x', m')\, d\left(\frac{x'}{\xi_0}\right) d\left(\frac{m'}{m_2}\right) \quad (30)$$

A suggested approximate solution to equation (30), derived in Appendix A, is analogous to equation (23):

$$n(x, m) \simeq K \exp\left[-\left(\frac{x}{\xi_0}\right)\frac{(m/m_2)^{g+1}}{g+1}\right] \quad (31)$$

and

$$m^2 n(x, m) \simeq K'\left(\frac{m}{m_2}\right)^2 \exp\left[-\left(\frac{x}{\xi_0}\right)\frac{(m/m_2)^{g+1}}{g+1}\right] \quad (32)$$

We emphasize that equation (31) is only an approximate solution and does not fully satisfy equation (30). The normalization (Figure 3) and distribution characteristics of equation (31) are given in Appendix B.

4. Volcanic Ash Analysis by SFT

We illustrate application of SFT to volcanic ash data by characterization of samples from four well-known tephra

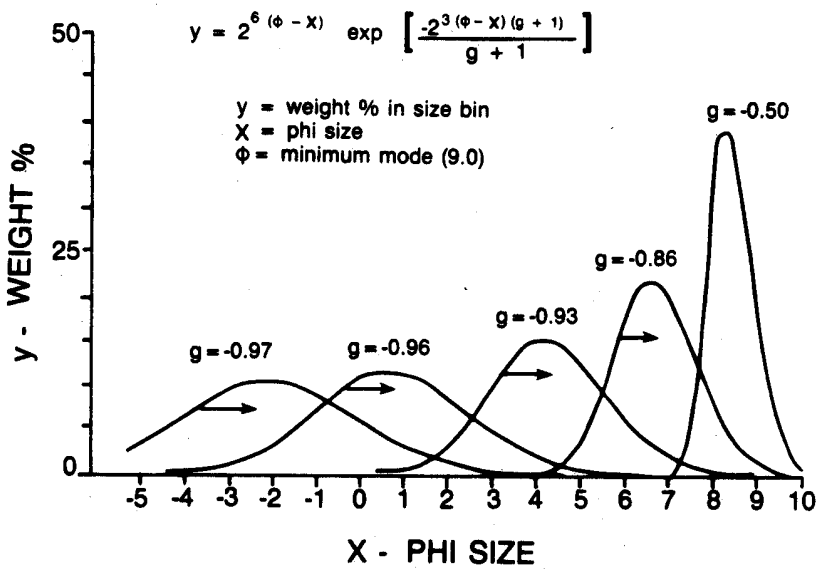

Fig. 4. Illustration of the transport distribution of the SFT. Curves show distributions for various values of g (γ) on a size-frequency histogram. For g near -1, the distribution is relatively coarser and flatter, but with increasing g values, which in general model increased processing and sorting, the distribution becomes finer and more peaked.

deposits: Mount St. Helens' 1980 debris avalanche [*Glicken*, 1986] and proximal bedded deposits, described by *Criswell* [1987], the Vesuvius AD 79 pumice fall [*Sigurdsson et al.*, 1985], Bishop Tuff pumice fall [*Sheridan*, 1965], and Crater Elegante pyroclastic-surge deposit [*Wohletz and Sheridan*, 1979]. These deposits represent a range of eruptive fragmentation mechanisms from magmatic [*Sparks*, 1978] to phreatomagmatic (hydrovolcanic) [*Wohletz*, 1983] and a variety of tephra transport modes, including fallout [*Carey and Sparks*, 1986], flow [*Sheridan*, 1979], and surge [*Wohletz and Sheridan*, 1979]. An important procedure in application of SFT is prior decomposition of polymodal distributions. The resulting data fit provided by SFT is shown to be generally superior to that afforded by the log normal distribution. In addition, characterization by SFT reveals fundamental particle size differences in these tephra deposits.

Geologic Illustration of the Free Parameters γ and g

The typical representation of geologic sieve data are histogram plots of size frequency, which show a general bell shape of the log normal distribution. For this representation, the sequential fragmentation/transport (SFT), $m^2n(m)$, distribution is similar to the log normal curve. It differs though by a variable skewness, controlled by the free parameter, γ or g, which in the range of interest for volcanic ash analyses generally produces a greater abundance of fines than is predicted by the log normal distribution. When γ (g) is very close to -1 the distribution is very wide and essentially flat where plotted on a size frequency histogram; the distribution is undefined and unbounded for $\gamma = -1$. An increase in γ (g) reflects increased comminution by a fragmentation mechanism and/or increased sorting by a transport mechanism. Figure 4 illustrates the form of the sequential transport distribution as g increases from -0.97 to -0.50.

Figure 5 provides a comparison of the sequential transport distribution to that of the log normal by three log normal curves with different standard deviations and the corresponding, best fitting sequential transport curves. Note that the sequential transport distributions more closely approximate the log normal ones as g approaches -1, as evidenced by the subtraction residuals of the two sets of curves.

The sequential fragmentation and sequential transport distributions are nearly identical in form when plotted on a size-frequency histogram (Figure 6). The only differences are that the sequential fragmentation distribution has slightly more of a skew in the fines (the coarse side of both distributions is governed by the argument of the exponent in equation (25), and the values of the free parameters γ and g vary by only a few percent for distribution with that parameter near -1.0). For more evolved (mature in a sedimentological sense) distributions that have a free parameter greater than about -0.2, the two distributions are nearly identical.

Application of SFT to Volcanic Ash

Geologic samples of volcanic ash do not generally represent the pristine distribution of particle sizes caused by the eruptive fragmentation mechanism. Samples obtained in the field have been processed by transport from the vent by one or a combination of transport processes, which include aerodynamically modified ballistic projection, atmospheric fallout, turbulent suspension, saltation, and traction flow. The size-sorting ability of these mechanisms modifies the pristine distribution and dictates application of the sequential transport formulation. As we shall discuss later, with application of the SFT the free parameter g in transport (analogous to γ for fragmentation) will vary depending upon the dominant transport mode. Because of the similarity of data fits between the transport and fragmentation distributions, we feel that in addition to learning about the transport history of individual samples, one can also characterize the fragmentation history by noting the nature of g for sample sets.

Volcanic ash particle size distribution data are usually found in the form $\Delta M/\Delta\phi$ where

$$\phi \equiv -\log_2 \left(\frac{l}{l_2} \right) \tag{33}$$

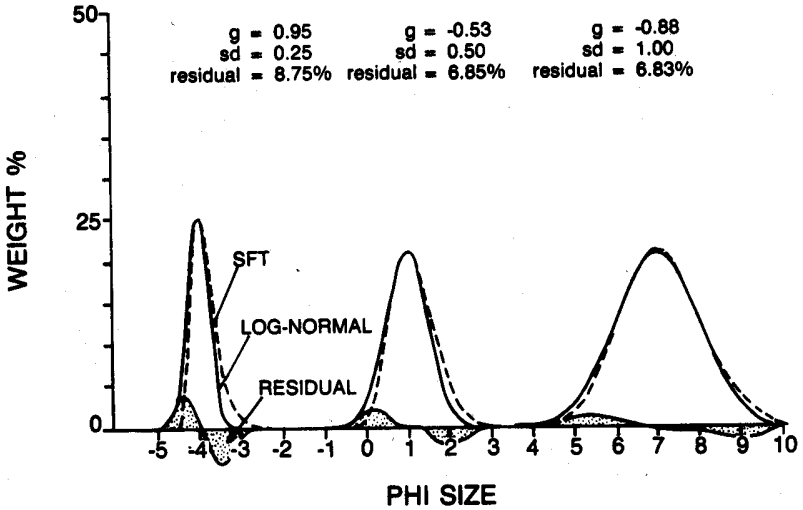

Fig. 5. Comparison on a size-frequency histogram of three log normal (Gaussian) distributions and corresponding, best fit SFT distribution. The difference between the two distributions for each curve is shown as a subtraction residual curve and areal difference in percent. Three log normal standard deviations and corresponding g (γ) values show that the two distributions become most similar for g near -1.

with $l_2 \equiv 1$ mm. We note that

$$\frac{dM}{d\phi} = -3 \ln (2) \frac{dM}{d \ln (m)} = -3 \ln (2) m^2 n(x, m) \qquad (34)$$

From these relationships it is clear that $dM/d\phi$ is a mass distribution, although it is usually plotted versus a logarithm scale in size. It is for this reason that in this and the previous section, we have discussed only mass distributions, converting from size where necessary. The reason that we emphasized the quantity $m^2 n(x, m)$ is now also clear from equation (B5), which cast in terms of particle diameter, assuming spherical particles, is

$$\frac{dM}{d\phi} = K_2 l^6 \exp \left[- \frac{x}{\xi_0} \frac{l^{3(g+1)}}{g+1} \right] \qquad (35)$$

For this representation K_2 is unity (for size-frequency histogram data [*Folk*, 1966]), $x/\xi_0 = 1$, as justified in equation (B9) and Figure 3, and particles are assumed to be of constant shape and density. These assumptions are other reasons why we have developed our model, based upon mass distributions, to circumvent the problem that volcanic ash is composed of crystal, rock, and glassy particles that vary in density and shape. In geologic application, we emphasize that one must consider the contributions of particles of varying density (e.g., separate the size distributions of principal constituents where a density contrast is significant). In light of these considerations, we show in Appendix C how equation (34) can be modified to take into account varying shape and density. The result of the modification upon the form of equation (35) is that $dM/d\phi$ becomes the summation of three terms all of the same form as the right-hand side of equation (35). This result demonstrates that the total distribution is polymodal with contributions of at least three subpopulations, all of the SFT form.

Because a change in the value for g in equation (35) produces a shift of the distribution peak, we define the shift

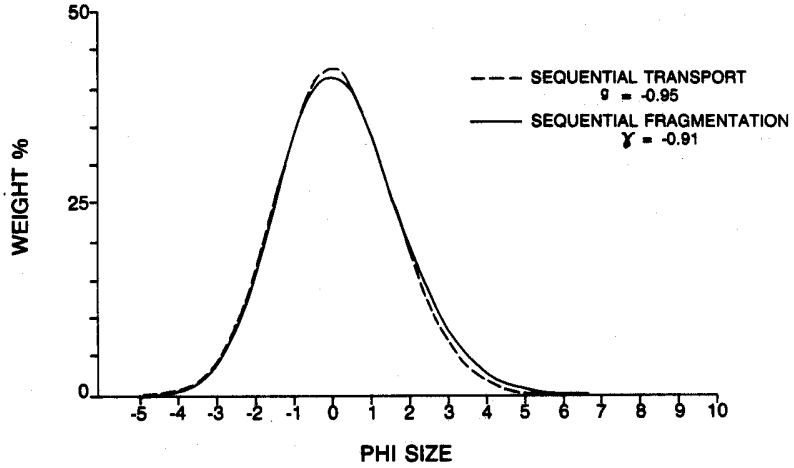

Fig. 6. Comparison showing the similarity of the sequential fragmentation and sequential transport distributions. Note that the coarse sides of the distributions are similar, but that the sequential fragmentation curve is finer skewed than the sequential transport curve even for larger γ (g) values.

as a function of g to facilitate the analysis in fitting data for which the peak location is known. The shift value is found by differentiating equation (35) with respect to l and finding l_p (the particle diameter at the distribution peak) where $dM/dl = 0$. The phi mode is the observed peak location (ϕ units) minus l_p, where $\log_2 l_p = [3(g + 1)]^{-1}$ for sequential transport, and $[1.443 \ln (\gamma + 2)][3(\gamma + 1)]^{-1}$ for sequential fragmentation, based upon differentiation of equation (25).

The standard deviation (in phi units) of this distribution given by equations (B5) and (33) is approximately

$$\sigma_\phi \simeq \frac{\text{FWHM}}{2\sqrt{2 \ln (2)}} \simeq \frac{0.340}{\sqrt{g+1}} + 0.006 \qquad (36)$$

where FWHM means the distribution's full width at its half maximum amplitude. The standard deviation is also independent of location x/ξ_0 (>0), and the above approximation is good to ± 1/4% ($-1 < g < -0.2$).

Decomposition of Polymodal Distributions

Sheridan et al. [1987] demonstrated the polymodality of size-frequency data for pyroclastic deposits, but an unbiased decomposition of subpopulations from data sets cannot be made with a distribution law, because the algorithm for decomposition assumes a subpopulation distribution form. Assuming that polymodal distributions are produced by mixtures of two or more subpopulations and that subpopulations exist in various proportions in all samples from a given sample set, we attempt to find the number of subpopulations, their individual forms, and the relative proportions of each comprising a tephra sample. Accordingly, we use the unmixing technique of *Ehrlich and Full* [1987], which provides a decomposition that is relatively free of mathematical bias. This technique employs a "vector analysis" because a correlation matrix is constructed in which sample data, transformed to multidimensional vectors, are represented by values in the matrix corresponding to the cosine of the angle between various pairs of data vectors. The minimum number of eigenvalues accounting for most of the variance (99% in our analysis) equals the number of components responsible for the original data set.

A set of 30 sample size analyses from Crater Elegante was chosen for subpopulation identification. EXTENDED CABFAC [*Klovan and Miesch*, 1976] was used for the vector analysis, and a QMODEL algorithm [*Full et al.*, 1982] provided supopulation compositions and mixing proportions for each sample of the set. This analysis, kindly provided by J. Horkowitz and R. Ehrlich of the University of South Carolina, is fundamentally different than that of factor analysis in that the data transformation used is completely reversible and provides unique results.

The results of the unmixing analysis show that six component or "endmember" subpopulations, combined in varying proportions, explain over 99% of the observed variance. These endmembers, illustrated in Figure 7, have varying skewness and are of no simple mathematical form. This result suggests that the physical process giving rise to the subpopulations is of complicated mathematical expression. Still, the skewness, displayed by some of the endmembers, supports an argument against fits, based upon a log normal distribution. A comparison of mathematical fits (Figure 8) of these empirical subpopulations demonstrates some advantage of the SFT over the log normal to characterize the data. Furthermore, the skewness of the endmembers resembles that produced by the SFT. In general, the SFT provides better fits to volcanic ash data than does the log normal distribution as is illustrated by Figures 9 and 10, which compare residuals obtained for the two alternatives.

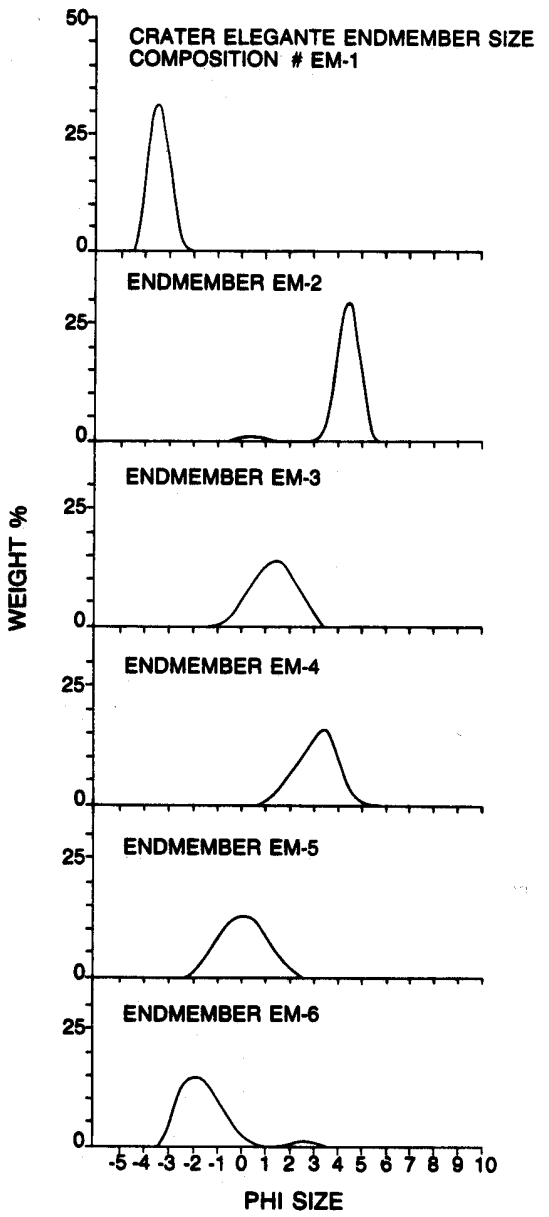

Fig. 7. Illustration of six endmember subpopulations derived from the principal component analysis of a set of 30 pyroclastic surge samples from crater Elegante, Mexico. Combination in various proportions of these endmembers explains over 99% of the observed variance in grain-size distribution. Note that the endmembers are of no prescribed mathematical form, but they do resemble both log normal and skewed SFT distributions.

Our conclusions from comparison of the SFT to the unmixed component distributions is that the SFT is appropriate for decomposition of polymodal size frequency distributions of volcanic ash. In order to analyze data, we have constructed an algorithm, "SEQUEN," for computer application, based upon an earlier log normal version, "GAUSS," [*Sheridan et al.*, 1987]. This algorithm allows user-interactive

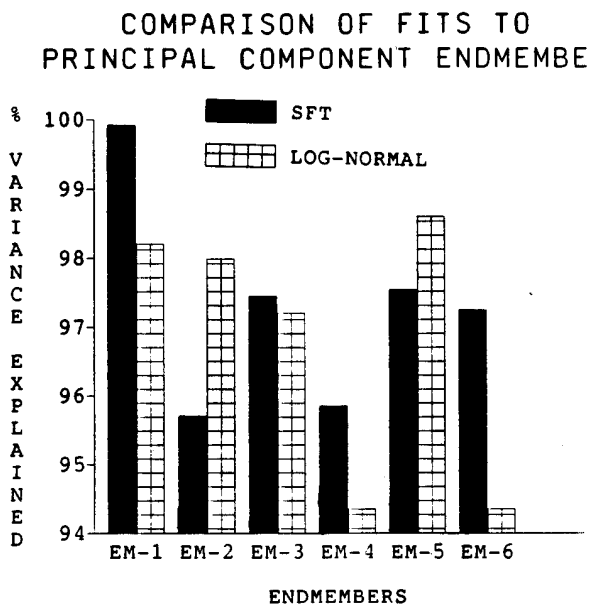

Fig. 8. Comparison of log normal and SFT fits to principal component endmembers. The plot shows that four of the six endmembers, the SFT explains more of the variance than does the log normal fit.

identification and characterization of SFT subpopulations from size-frequency data using equation (35). The characterization provides the mode, gamma or g, and proportion of each subpopulation, as well as the goodness-of-fit for the total sample.

Data Analysis

Figure 11 illustrates results of five example data fits using SEQUEN. For each example, data points are compared to the curve resulting from the SFT fit. Note the characterization of the SFT subpopulations required to produce the fit. Below each comparison plot, the decomposed subpopulations are plotted with respect to the cubic spline curve passing through each original data point. Besides the polymodal character of these various types of volcanic ash samples and the goodness-of-fit shown by the SFT model, the typical skewness of the original distributions is apparent. Skewing of fines has been the reason previous workers were dissatisfied by log normal characterizations. One example though, the Bishop Tuff fall (Figure 11*b*) shows an overall coarse skewing that we modeled as a result of superposition of two subpopulations. This fit is somewhat arbitrary in that perhaps one coarsely skewed population might provide an adequate characterization; however, we prefer the polymodal fit based upon consideration of the tephra fallout mechanism to be discussed later.

A general application of the SFT model is comparison of the results obtained for each of the four example tephra sample sets. Figure 12 is a histogram of subpopulation mode frequencies that contribute over 30% to their respective sample distributions. Within the limited data set, the avalanche deposits (MSH A) contain the coarsest subpopulations and the phreatomagmatic deposits (CE) the finest. The proximal bedded tephra (MSH PBD) is generally finer than fallout tephra (FALL) but shows a smaller range of modes than does the phreatomagmatic tephra. This comparison

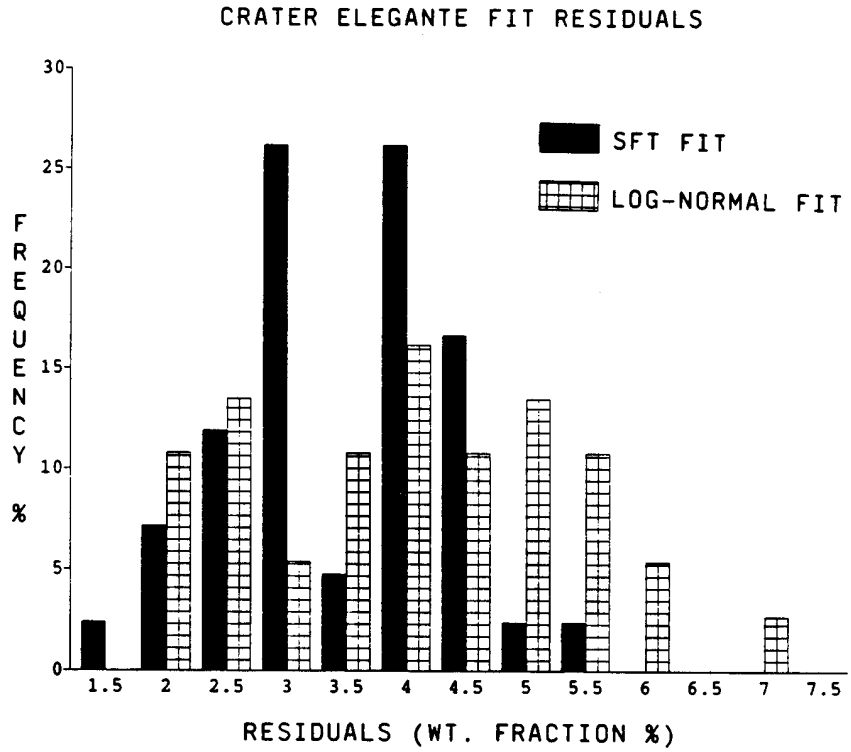

Fig. 9. Comparison of SFT and log normal fits to Crater Elegante samples. The SFT fits result in less than 5.5% residual (calculated by least squares fit of data to the theoretical curve) and overall are better than the log normal data fits.

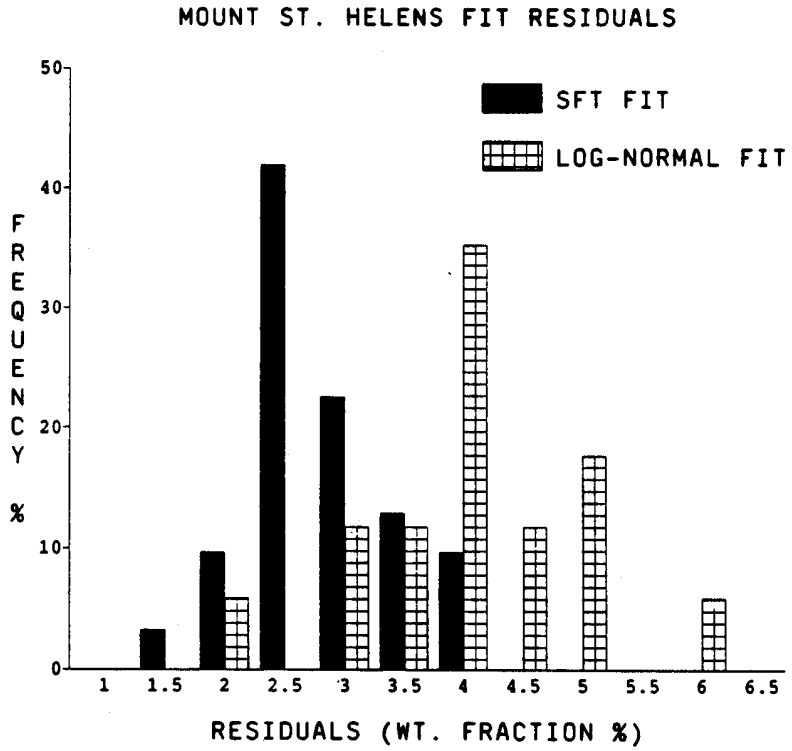

Fig. 10. Comparison of SFT and log normal fits to Mount St. Helens ash samples. SFT residuals are less than 4%, again much better than those produced by the log normal.

supports our formulation that different fragmentation and transport mechanisms develop different mass distributions.

Figures 13–15 are data plots for the four analyzed sample sets, and they show comparison of subpopulation parameters obtained from the analysis: (1) weight fraction versus phi mode (Figure 13); (2) weight fraction versus g (Figure 14); (3) g versus phi mode (Figure 15). Although these figures show a considerable scatter of data, we have fitted least squares regression curves in order to establish data trends. We believe that these trends would be much better defined for data sets from controlled sampling (e.g., single sample localities). Of greatest interest are plots showing behavior of g. Inspection of Figures 14 and 15 shows several interesting data trends: (1) for surge, avalanche, and flow deposits of Crater Elegante and Mount St. Helens, the tendency shows most sample modes having g values less than –0.75 and a general exponential decrease in weight fraction of modes for increasing g (Figure 14); (2) this same trend is noted for Bishop fallout ash, but the opposite is shown for samples of Vesuvius fall; (3) g values are most positive for coarse and fine modes for all samples except the fall deposits (Figure 15), the variation of g fits a power law of phi mode, and again there is a difference noted for the behaviors of the Bishop and Vesuvius samples.

5. Discussion

We prefer the SFT model for applications to volcanic ash data, because it is suitable for a physical analysis. The theory is very basic and is expressed for fragmentation and transport processes by equations (21) and (29), respectively. These equations implicitly show the underlying dependence of particle-mass distributions upon physical process. Although different functional forms of mass dependency can be postulated, the power law forms of equations (21) and (29) produce good fits to observed data. Analyses of fragmentation and transport physics, based upon Newtonian mechanics, can be developed from expressions of continuity, momentum, and energy, all of which require consideration of mass. In simplified form such analyses allow prediction of values of γ and g for the above equations. More detailed analysis relates these free parameters to recurrent phenomena involved. With respect to this latter consideration, one can think of the significance of these free parameters as measures of sample processing, a concept easily visualized for ball-milling or multiple stages of transport and deposition. The following discussion does not aim at developing the detailed physics of fragmentation and transport. Using previous analyses of such processes, we show how the SFT model can be incorporated.

Fragmentation

Volcanic ash can be formed in volcanoes by many different processes that transform large batches of magma and country rock into smaller pieces. Two general mechanisms are (1) magmatic fragmentation in which exsolution and expansion of magmatic gases contribute to volcanic ash production, and (2) hydrovolcanic fragmentation in which physical contact and mixing of magma with external water results in ash formation. In both cases, the number fragments of a specified size range will be indirectly proportional to the mass of those fragments, which in turn is governed by the single-event fragmentation function (equation (21)) of the fragmentation process.

Magmatic fragmentation is generally marked by the pres-

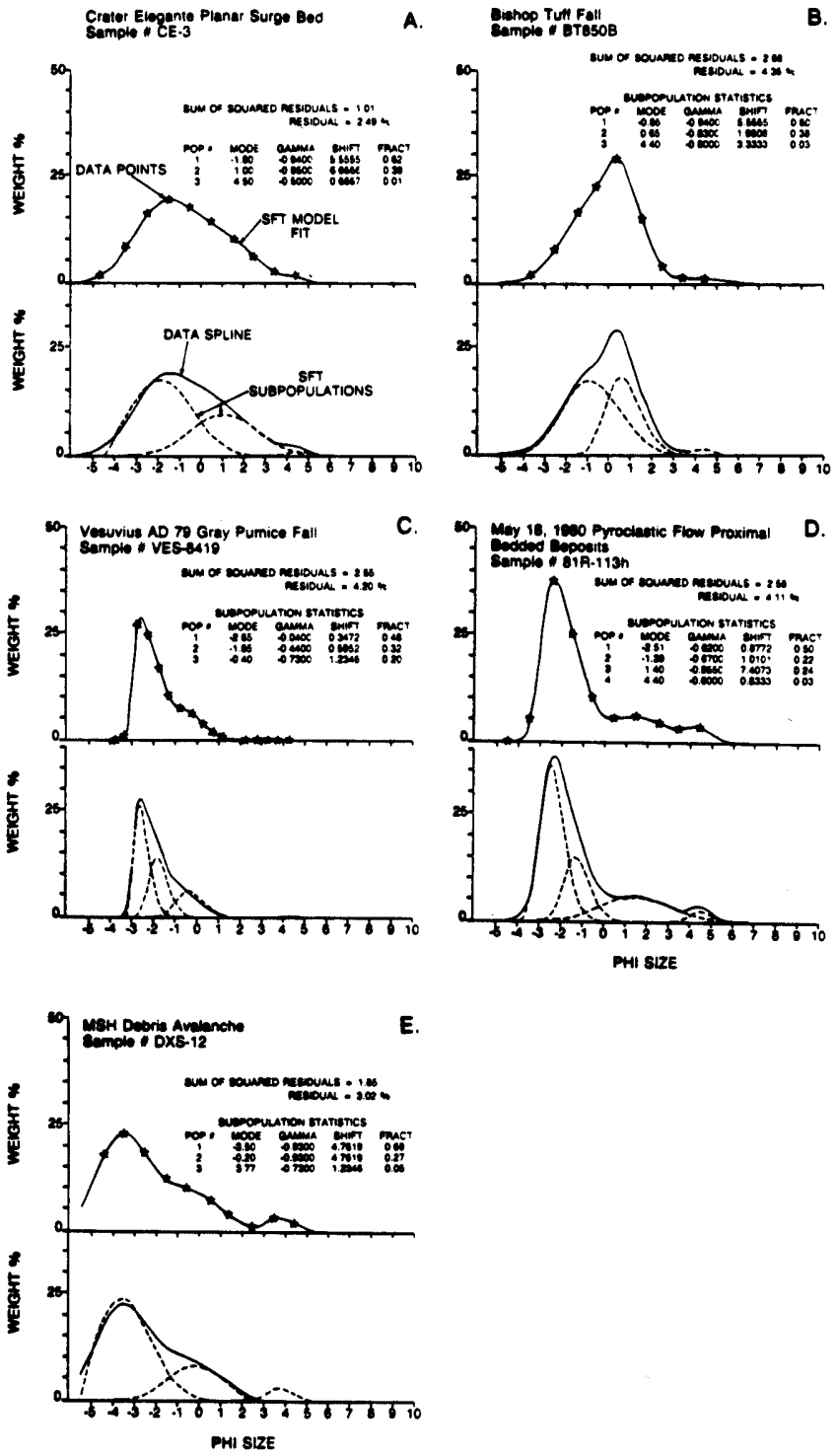

Fig. 11. Plots showing example data fits using the SFT. Each plot shows original data points, fit produced by SFT analysis, subpopulation characteristics, and comparison of subpopulation distributions to the data spline distribution. (*a*) Crater Elegante planar pyroclastic surge bed. (*b*) Bishop Tuff ash fall sample. (*c*) Vesuvius AD 79 gray pumice fall sample. (*d*) Mount St. Helens proximal bedded deposit sample. (*e*) Mount St. Helens debris avalanche sample.

ence of vesicles in volcanic ash and production of pumice. *Sparks* [1978] models the growth of vesicles in magma and shows that where their growth exceeds an estimated volume limit for a magma, the magma breaks apart at vesicle intersections. This model is complicated by the movement of stress waves within the magma as it approaches the surface of the Earth beneath a volcano. Expansion waves of sufficient amplitude are expected to exceed the bulk modulus of the magma causing its failure in tension [*Wohletz et al.*, 1984]. For stress wave propagation, the sizes of ash particles formed by the magmatic mechanism are thought to be functions of the initial size distribution of planes of weakness

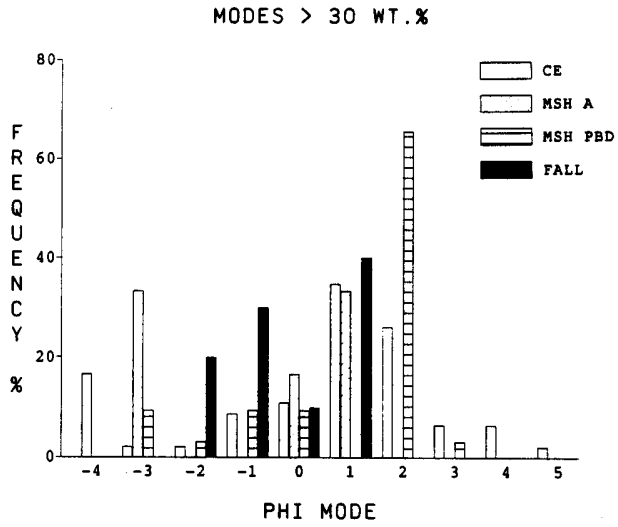

Fig. 12. Histogram of principal subpopulation modes for the four sample sets: CE, Crater Elegante; MSH A, Mount St. Helens debris avalanche; MSH PBD, Mount St. Helens proximal bedded deposits; FALL, Bishop Tuff fallout and Vesuvius AD 79 fallout.

within the magma such as vesicle [*Whitham and Sparks*, 1986] and crystal surfaces [*Cashman*, 1986]. With respect to vesicles, *Sparks and Brazier* [1982] document a polymodal distribution of sizes, which might be reflected in polymodal distribution after fragmentation. In addition, *Heiken and Wohletz* [1985] illustrate the nucleation of vesicles on crystal faces, which suggests that the two kinds of structural weaknesses, crystal surfaces and vesicles, can be related. The sizes of these features are directly proportional to mass to the one-third power (volume limitation) and mass to the two-thirds power (area dependence). In both cases the number of particles formed of a given size range is indirectly proportional to sizes as mentioned above; hence γ is expected to be between $-1/3$ and $-2/3$ for fully developed magmatic fragmentations. Note that if the fragmentation mechanism does not fully evolve, γ will remain near -1.

Hydrovolcanic (phreatomagmatic) fragmentation occurs where magma comes into contact with external water. Several mechanisms can account for magma fragmentation as outlined by *Wohletz* [1983, 1986]. As with the magmatic case, propagation of stress waves through the magma, caused by the magma's unloading in the crater, is expected to contribute to fragmentation. Also contributing to hydrovolcanic ash production are instabilities that develop at interfaces between magma and water and grow during expansion of vapor films. For growth of instabilities, *Wohletz* [1986] shows that surface tension is an important limiting parameter for instability wavelength and resulting fragment size. In this case, fragment size is directly proportional to mass to the 1/2 power. During vapor expansion and explosion, *Wohletz* [1986] shows that final particle size is directly related to surface tension (surface tension directly proportional to mass) and indirectly related to magma-water relative velocities squared. Assuming the relative velocity varies as a function of particle drag, fragment size is proportional to mass to the $-1/3$ power. Hence γ is expected to be between $-1/2$ and 1/3 for hydrovolcanic fragmentations.

To illustrate the above general applications of sequential fragmentation to volcanic ash, we fit the distribution to

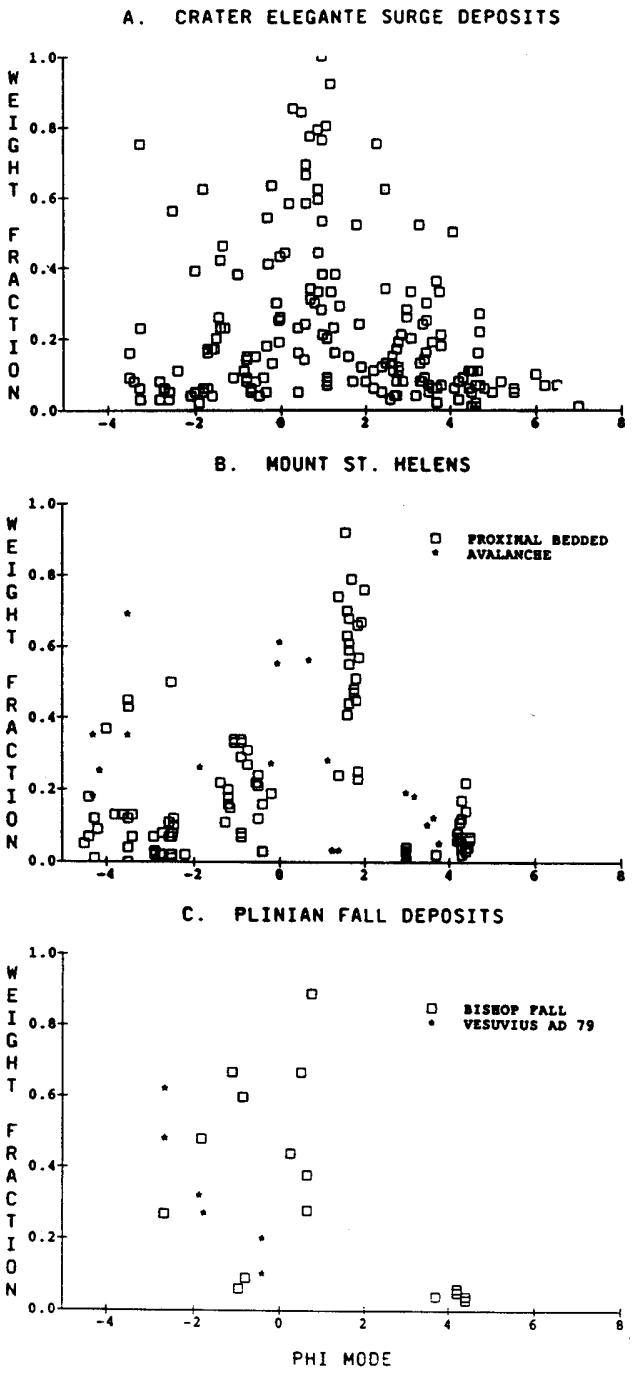

Fig. 13. Plots of subpopulation weight fraction versus subpopulation mode. (*a*) Crater Elegante, (*b*) Mount St. Helens, (*c*) Plinian fall deposits from Bishop Tuff and Vesuvius AD 79 fall.

samples that represent hydrovolcanic and magmatic fragmentations. Samples include those from Crater Elegante, a predominantly phreatomagmatic maar volcano in Sonora, Mexico, and samples of ash from Mount St. Helens recent pumice eruptions, some of which are demonstrably magmatic [*Eichelberger and Hayes*, 1982]. Figure 16 is a histogram of γ values for these two sample sets. It is apparent that the phreatomagmatic samples have a much wider range in γ (-1.0 to 1.1; average $\gamma = -0.50$) than do the magmatic ones ($-1.0 < \gamma < -0.3$; average $\gamma = -0.72$). This result is in

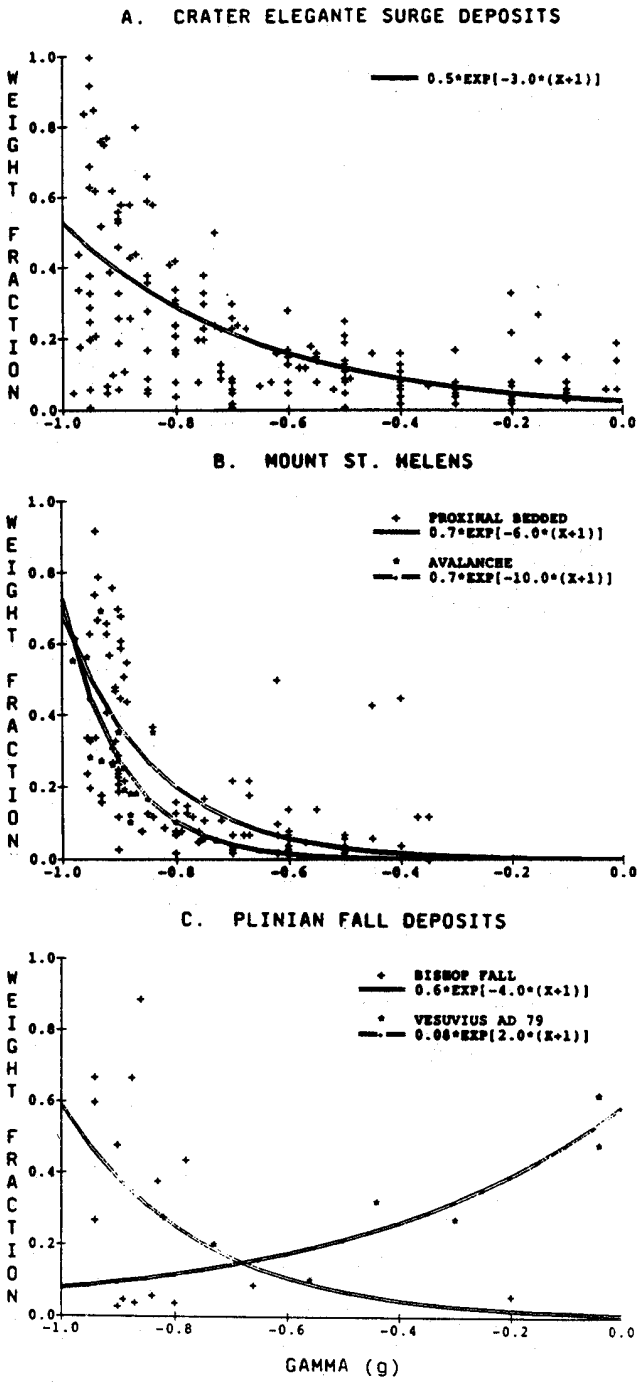

Fig. 14. Plots of subpopulation weight fraction versus subpopulation g value. (*a*) Crater Elegante, (*b*) Mount St. Helens, (*c*) Plinian fall deposits from Bishop Tuff and Vesuvius AD 79 fall. Note fitted curves shown only to highlight general data trend.

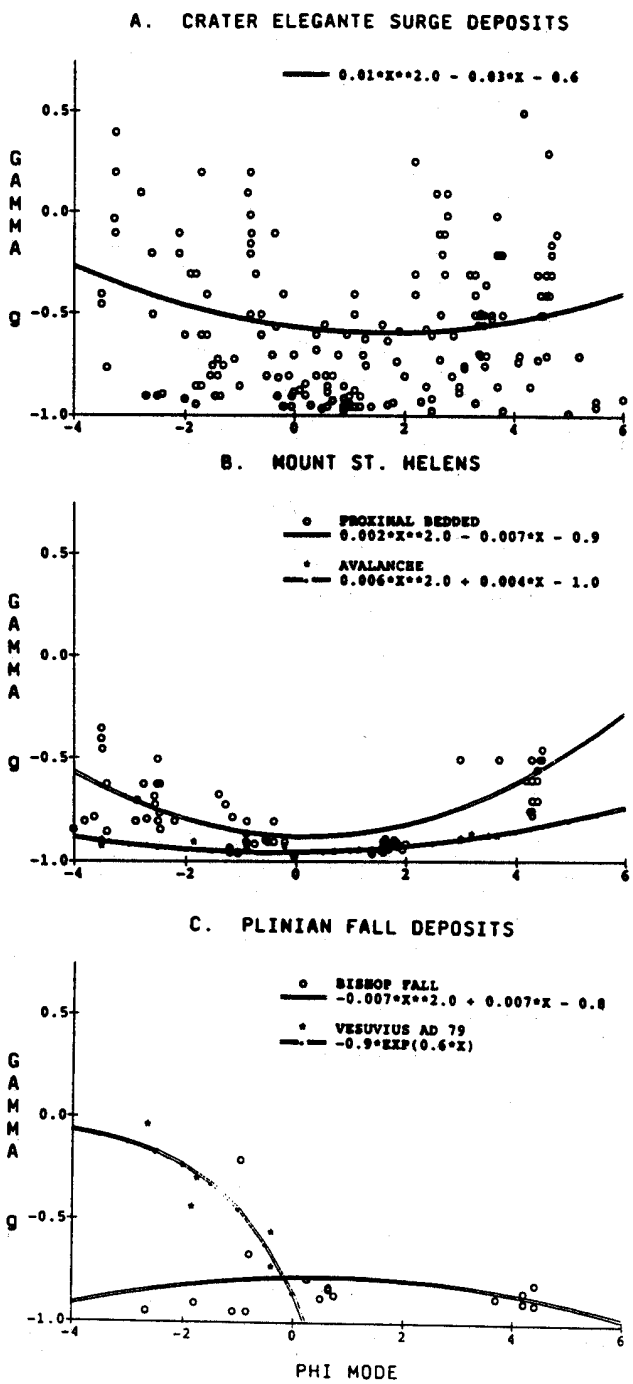

Fig. 15. Plots of subpopulation g value versus subpopulation mode. (*a*) Crater Elegante, (*b*) Mount St. Helens, (*c*) Plinian fall deposits from Bishop Tuff and Vesuvius AD 79 fall. Note fitted curves shown only to highlight general data trend.

general what we predict above. We note that the ranges in γ, however, are broadened by overprinting of transport processes and that the Crater Elegante samples may have a small magmatic component.

Interpretations of fragmentation mechanisms for these samples from Crater Elegante and Mount St. Helens can be extended to estimates of initial fragment sizes prior to eruptive fragmentation. For the former samples, Figure 15*a* shows coarse population modes near -4ϕ (16 mm). Because the lowest γ values observed for those samples ($\gamma = -0.95$) reflect initial distribution locations, the Crater Elegante coarse population modes experienced a fine shift of about 6.2 ϕ, such that initial fragment sizes were in the range of meter-sized blocks prior to fragmentation. For the Mount St. Helens samples (Figure 15*b*) the coarse modes have γ values that reflect fine shifts of only about 4.6 ϕ from initial peak locations determined by lowest observed γ at -0.94; initial sizes determined by vesicle and crystal planes of weakness

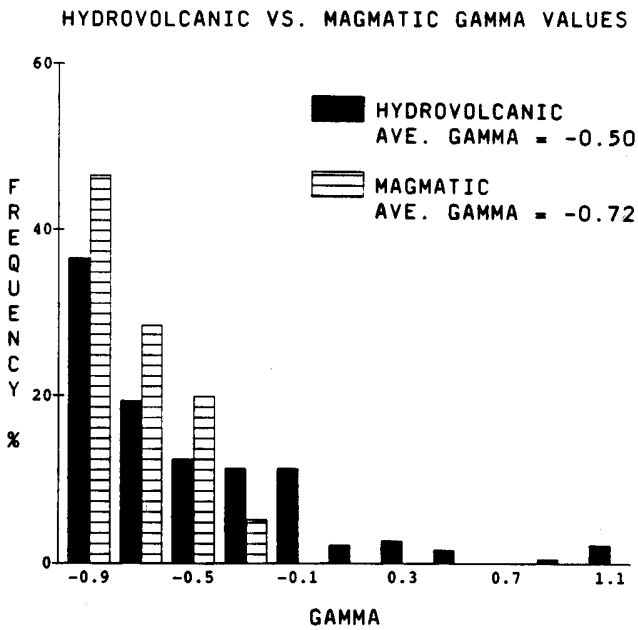

Fig. 16. Histogram of observed gamma values for samples of hydrovolcanic (Crater Elegante) and magmatic (Mount St. Helens) fragmentation origins, as interpreted from geologic relationships. Hydrovolcanic sample gamma values show a much wider range than do those of magmatic samples, as predicted.

would have been only in the range of centimeters. These predictions are consistent with a hydrovolcanic origin for Crater Elegante samples in contrast to a magmatic origin for the pumiceous samples of Mount St. Helens.

Transport

Processes responsible for transport of volcanic ash from the crater to sites of deposition and sampling are suspension in and fallout from the atmosphere (water for submarine eruptions), and lateral moving flows that interact with the substrate. These processes are generalized, but in the following analysis, we assume the number of particles of a given mass accumulating at some sample range is proportional to the transport range, which is a function of mass (equation (29)). For the fallout case, ballistic and suspension processes operate, whereas in the case of lateral transport, particle hopping (saltation) and rolling (traction) also must be considered.

For ballistic transport, the aerodynamic drag affecting particles increases with decreasing size, and it strongly determines the range for particles smaller than several centimeters [*Schultz and Gault*, 1979]. For large particles, transport range is directly proportional to launch velocity, which is in turn proportional to mass to the $-1/2$ power. Because drag is a function of surface area, small particles are expected to show a modified ballistic range indirectly proportional to mass to the $-1/3$ power, as shown in the solutions to the equations of motion derived by *Wilson* [1972]. For very fine particles, suspended transport causes range to be directly related to fallout times, which are determined surface area such that range increases with mass to the $-2/3$ power. Values of g (γ) for fallout ash are expected to vary from $-2/3$ to $-1/3$.

Volcanic ash transported in pyroclastic flows and surges can experience significant transport by saltation and traction movement [*Denlinger*, 1987]. In cases of saltation and traction movement analysis of mass dependency is very complicated. The threshold velocity between rolling and hopping is shown by *Bagnold* [1941] to be proportional to mass to the 1/6 power, such that range is expected to increase with mass to the $-1/6$ power. *White* [1979] extended the analysis and computed saltation path length, as a function of lift-off speeds, to be proportional to mass approximately taken to the $-1/2$ to $-2/3$ power. Thus a range of g is approximated for saltation transport as $-2/3 < g < -1/6$. In support of our transport model, *Anderson and Hallet* [1986] in fact propose a two-parameter gamma function fit to *White and Schulz*'s [1977] experimental measurements of saltation lift-off speeds. Where lateral transport velocities are too small to lift particles, traction movement can be calculated as a function of shear stress and rolling friction. Thus transport range for constant shear velocity is indirectly proportional to the square root of mass to the two-thirds power and indirectly proportional to mass to the one-third power. Values of g are then expected to be near $-2/3$ for these cases.

In consideration of transport effects upon g, we compare g as a function of deposit types, including surge, debris avalanche, fallout, and pyroclastic flow samples discussed above (Figures 14 and 15). It is evident, as discussed above, that correlation exists among these parameters, which is support for interpretation that data trends can be related to underlying physical processes. On the other hand, each sample can be interpreted on an individual basis as to the significance of g. Because the coarse and fine modes show relatively higher gamma values in Figures 15*a* and 15*b*, we believe that these modes reflect fragmentation/transport processes, interpreted as ballistic and suspension modes [*Sheridan et al.*, 1987], which are more evolved than those responsible for the intermediate subpopulations (traction and saltation modes).

Another test of the effect of transport process upon g is a comparison of observed g values for sample subpopulations in which the responsible process can be determined by deposit characteristics. *Sheridan et al.* [1987] also show that sample subpopulations can be assigned to a likely transport process in pyroclastic surge deposits by considering experimental wind tunnel data. In essence, coarse subpopulations ($l > 2$ mm) are associated with samples from deposits whose bedding features are characteristic of ash fall, finer subpopulation from samples taken from planar-bedded and dune-bedded deposits can be attributed to traction and saltation transport processes respectively, while the finest subpopulations ($l < 0.125$ mm) are considered to be dominantly transported by suspension. Figure 17 shows the ranges of g values observed for Crater Elegante samples where bed forms and textures constrain likely transport processes. We note that average values of g for the transport processes considered fall within the ranges predicted above, which supports the hypothesis that g is a function of transport mechanism.

Table 1 outlines various fragmentation and transport mechanisms and possible expected ranges of γ and g. The ranges estimated for these various fragmentation/transport processes show overlap, which rules out unique interpretations based upon model parameters. One must consider each mechanism separately as to the number of sequential steps likely to be involved in the process. We emphasize that

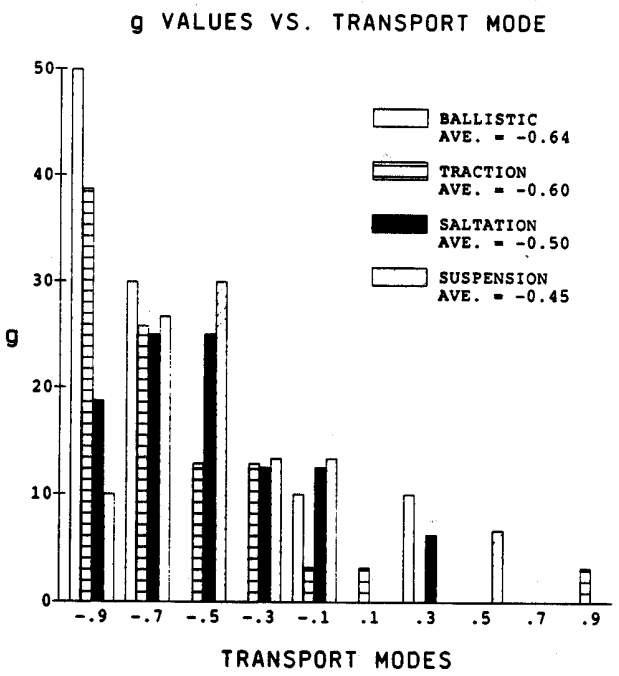

Fig. 17. Histogram of g values observed for Crater Elegante samples where subpopulations can be assigned to a specific transport process using the analysis of *Sheridan et al.* [1987]. Average g values for each transport process can be compared to predicted values shown in Table 1.

values in this table are tentative, and that with detailed analysis of physical processes involved with formation and dispersal of volcanic ash, much more accurate ranges of g and γ can be formulated.

6. Conclusions

In conclusion, we have found that the SFT particle-size distribution provides better fits to volcanic ash data than does the log normal distribution. In deriving the SFT distribution we have shown that it is physically related to processes sensitive to mass. Because of this physical basis, we believe the SFT model will allow much greater interpretation of volcanic ash size-frequency distributions, especially with respect to formative and transport processes. Although the SFT appears to apply to wide range of geophysical and astrophysical data sets concerning size distributions of fragmental materials, the theory has not yet been tested on well-known geological occurrences such as marine and fluvial sediments. Further development of this model with respect to interpretation of data sets could benefit from application to experimentally derived data sets.

Appendix A: An Approximate Solution to the Transport Equation (30)

Equation (30), developed in the text of this article, is

$$n(x, m) = \int_0^{m/m_2} \left(\frac{m'}{m_2}\right)^g \int_{(x-\xi)/\xi_0}^0 n(x', m')\, d\left(\frac{x'}{\xi_0}\right) d\left(\frac{m'}{m_2}\right) \tag{A1}$$

We have found no exact solution to equation (A1) in terms of ordinary functions. What follows is therefore an attempt to derive an approximate solution that possesses qualities that are useful in describing data.

The first difficulty that we recognize is that although $n(x, m)$ is assumed to be a continuous function in x, there is in fact a discontinuity in $n(x, m)$ at the edge of the source pile ($x = 0$). This discontinuity is only finite at the initial stage of transport and vanishes for late steps in sequential transport; its effect is minimal for locations $x > 0$. Accordingly, we ignore the initial discontinuity in order to find an approximate solution.

Differentiating equation (A1) with respect to m, we obtain

$$\frac{dn(x, m)}{d(m/m_2)} = \left(\frac{m}{m_2}\right)^g \int_{(x-\xi)/\xi_0}^0 n(x', m)\, d\left(\frac{x'}{\xi_0}\right) \tag{A2}$$

We then differentiate with respect to x and find that

$$\frac{d^2n(x, m)}{d(x/\xi_0)d(m/m_2)} = \left(\frac{m}{m_2}\right)^g \left[-n\left(\frac{x-\xi}{\xi_0}, m\right)\right] \tag{A3}$$

The second difficulty is now clear: there is a discrepancy in the argument of x in the function n. Again, in the interest of proceeding to an approximate solution, we ignore this inconsistency. Rearranging equation (A3), we obtain

$$\frac{d^2n}{n} = -\left(\frac{m}{m_2}\right)^g d\left(\frac{m}{m_2}\right) d\left(\frac{x}{\xi_0}\right) \tag{A4}$$

To simplify the left-hand side of this equation, we now note that

TABLE 1. Possible variation of γ and g With Fragmentation and Transport Processes

	γ (g)							
Process	−1.0	−0.80	−0.60	−0.40	−0.20	0.0	0.20	0.40
Fragmentation								
Magmatic		----------x----------						
Hydrovolcanic				--x ----------				
Transport								
Ballistic*		----------x----------						
Suspension			----------x----------					
Saltation			------x ----------					
Traction			----------x----------					

Processes are generalized for range of physical mechanisms involved. Observed values of γ and g are denoted by cross.
*Ballistic transport for fragments larger than 1 mm.

$$d\left(\frac{dn}{n}\right) = \frac{nd^2n - (dn)^2}{n^2} = \frac{d^2n}{n} - \frac{(dn)^2}{n^2} \tag{A5}$$

Because $(dn)^2/n^2 << d^2n/n$, we can neglect the squared differential to obtain the following approximation.

$$\frac{d^2n}{n} \simeq d\left(\frac{dn}{n}\right) \tag{A6}$$

Using equation (A6), equation (A4) becomes

$$d\left(\frac{dn}{n}\right) \simeq -\left(\frac{m}{m_2}\right)^g d\left(\frac{m}{m_2}\right) d\left(\frac{x}{\xi_0}\right) \tag{A7}$$

Twice integrating equation (A7) gives

$$\ln (n) \simeq \frac{x}{\xi_0}\left[\frac{(m/m_2)^{g+1}}{g+1}\right] \tag{A8}$$

Taking the exponential form of this equation,

$$n(x, m) \simeq K \exp\left[-\left(\frac{x}{\xi_0}\right)\frac{(m/m_2)^{g+1}}{g+1}\right] \tag{A9}$$

where K is a constant of integration. We stress that we have derived only an approximate solution to equation (A1), as can be verified by substitution of equation (A9) back into equation (A1); to the best of our knowledge, the general transport equation (26) has no exact solution. We note that $n(x, m)$ grows exponentially large for $x < 0$, but the contribution from the source pile at large negative x is minimal. In any case, we will limit our attention to locations $x > 0$.

APPENDIX B: NORMALIZATION AND INTEGRAL FORMS OF EQUATION (31)

To normalize the distribution of equation (31) and thus find K, we take

$$N_t = \int_0^\infty \int_0^\infty n(x, m)\, dx\, dm \tag{B1}$$

Owing to the approximate nature of equation (31), we cannot perform both of the integrations indicated in equation (B1). Inserting equation (31) in equation (B1) and integrating only with respect to m, we find that

$$N_t(x) = Km_2(g+1)^{-g/(g+1)}\Gamma\left(\frac{1}{g+1}\right)\left(\frac{x}{\xi_0}\right)^{1/(g+1)} \tag{B2}$$

where $\Gamma(\varepsilon)$ is the complete gamma function, defined by

$$\Gamma(\varepsilon) \equiv \int_0^\infty t^{\varepsilon-1}e^{-t}\, dt \tag{B3}$$

Equation (B2) indicates that for any particular value of g, the total number of transported particles (per unit length) decreases by a power law with increasing distance from the edge of the source pile. $N_t(x)\, dx$ integrated from 0 to ∞ is undefined. Under these circumstances, we have chosen to retain K as a constant. Then the mass distribution is given by

$$mn(x, m) = Km_2\left(\frac{m}{m_2}\right)\exp\left[-\frac{x}{\xi_0}\frac{(m/m_2)^{g+1}}{g+1}\right] \tag{B4}$$

The mass distribution per unit ln (m) interval is

$$m^2n(x, m) = Km_2^2\left(\frac{m}{m_2}\right)^2\exp\left[-\frac{x}{\xi_0}\frac{(m/m_2)^{g+1}}{g+1}\right] \tag{B5}$$

As we shall see, at any location x/ξ_o, equation (B5) is quite similar to a log normal distribution. In fact, it varies only slightly from the fragmentation equation, which in analogous form has a factor of γ in the exponents for the masses in front of the exponent [*Brown*, 1989]. Because the argument of the exponent controls the coarse side of the distribution and is identical for the fragmentation transport equations, the only difference between the two is that the former has slightly more skewing in the fine side of the distribution.

By differentiating equation (B5) with respect to the fragment mass and setting the result equal to zero, one finds the location of the distribution peak, m_p, to be

$$\frac{m_p}{m_2} = 2^{1/(g+1)}\left(\frac{x}{\xi_0}\right)^{-1/(g+1)} \tag{B6}$$

This equation gives the most probable mass of the distribution, which is also called the mode. It can be seen that for $g > -1$, as the distance from the edge of the source pile increases, the peak shifts toward lower masses.

The average mass, $\bar{m}$, is found by setting

$$\bar{m} = \frac{M_t}{N_t} = \frac{\int_0^\infty m^2n(x, m)\, d\ln(m)}{\int_0^\infty n(x, m)\, dm} \tag{B7}$$

Inserting equations (30) and (B5) into equation (B7), we find that

$$\frac{\bar{m}}{m_2} = (g+1)^{1/(g+1)}\frac{\Gamma(2/(g+1))}{\Gamma(1/((g+1))}\left(\frac{x}{\xi_0}\right)^{-1/(g+1)} \tag{B8}$$

From equation (B8) it can be seen that, as in the case of the peak location, for $g > -1$ the average mass decreases with increasing distance from the pile, and with the same functional dependence. Thus the distance x/ξ_o may be eliminated between equations (B6) and (B8) to give

$$\frac{\bar{m}}{m_p} = \left(\frac{g+1}{2}\right)^{1/(g+1)}\frac{\Gamma(2/(g+1))}{\Gamma(1/(g+1))} \tag{B9}$$

which is a fixed ratio for any particular value of g. Equation (B9) shows that the shape of the distribution curves is not a function of x/ξ_0 but only of g. This relationship is easily verified by choosing a value of g and plotting the distribution of equations (31), (B4), or (B5) for various locations of x/ξ_0 (Figure 3).

The integral number distribution (at any location x/ξ_0) is given by

$$\frac{N(>m)}{N_t} \equiv \frac{\int_m^\infty n(x, m)\, d(m)}{\int_0^\infty n(x, m)\, dm} \tag{B10}$$

To find this function for the transport distribution, one needs the definition of the complementary, incomplete gamma function, i.e.,

$$\Gamma(\varepsilon, z) \equiv \int_z^\infty t^{\varepsilon - 1} e^{-t}\, dt \tag{B11}$$

This is a standard computer library resource, and it is often called "GAMIC." Defining

$$z \equiv \left(\frac{x}{\xi_0}\right) \frac{(m/m_2)^{g+1}}{g+1} \tag{B12}$$

and substituting equation (31) in equation (B10), one finds that

$$\frac{N(>m)}{N_t} = \frac{\Gamma(1/(g+1), z)}{\Gamma(1/(g+1))} \tag{B13}$$

With definition of the incomplete gamma function ("GAMI")

$$\Upsilon(\varepsilon, z) \equiv \int_0^z t^{\varepsilon - 1} e^{-t}\, dt \tag{B14}$$

and noting that

$$\Upsilon(\varepsilon, z) + \Gamma(\varepsilon, z) = \Gamma(\varepsilon) \tag{B15}$$

one obtains

$$\frac{N(<m)}{N_t} = 1 - \frac{N(>m)}{N_t} = 1 - \frac{\Gamma(1/(g+1), z)}{\Gamma(1/(g+1))} = \frac{\Upsilon(1/(g+1), z)}{\Gamma(1/(g+1))} \tag{B16}$$

The integral mass distribution is then given by

$$\frac{M(<m)}{M_t} \equiv \frac{\int_0^m m^2 n(x, m)\, d \ln (m)}{\int_0^\infty m^2 n(x, m)\, d \ln (m)} \tag{B17}$$

Substituting equation (B5) into equation (B17), we find that for our particle transport theory

$$\frac{M(<m)}{M_t} = \frac{\Upsilon(2/g+1), z)}{\Gamma(2/(g+1))} \tag{B18}$$

Also,

$$\frac{M(>m)}{M_t} = 1 - \frac{M(<m)}{M_t} = 1 - \frac{\Upsilon(2/(g+1), z)}{\Gamma(2/(g+1))} = \frac{\Gamma(2/(g+1), z)}{\Gamma(2/(g+1))} \tag{B19}$$

APPENDIX C: EFFECTS OF VARYING PARTICLE SHAPE AND DENSITY

The mass of a particle can be simply expressed as

$$m = \frac{4}{3}\pi S \rho \left(\frac{l}{2}\right)^3 \tag{C1}$$

for which S is a shape factor often defined as $S = P^2/(4\pi A_r)$, where P is the perimeter and A_r is the area. Because most volcanic ash size measurements are obtained by sieving, l is usually the smallest diameter of a particle passing through a sieve screen, and S is generally greater than unity, such that the true mass of a nonspherical particle is generally greater than that calculated if it is assumed to be a sphere of diameter l.

Our approach to considering the effect of shape and density variations upon the total mass per size interval, $dM/d\phi$, is to formulate S and ρ as functions of ϕ, as is generally found by microscopic inspection of volcanic ash samples [*Walker*, 1971]. Taking the logarithmic form of equation (C1),

$$\ln (m) = \ln (4\pi/3) + \ln (S) + \ln (\rho) + 3[\ln (l) - \ln (2)] \tag{C2}$$

and then differentiating with respect to ln (l), we obtain

$$\frac{dm}{d \ln (l)} = \frac{m d \ln (S)}{d \ln (l)} + \frac{m d \ln (\rho)}{d \ln (l)} + 3m \tag{C3}$$

Because $d \ln (l) = -\ln (2)\, d\phi$, we can write an equation analogous to equation (34), except it includes the differential effects of shape and density:

$$\frac{dM}{d\phi} = -m^2 n(x, m)\left[3 \ln (2) + \frac{dS}{S d\phi} + \frac{d\rho}{\rho d\phi}\right] \tag{C4}$$

From inspection of ash constituent (e.g., rock fragments, pumice, crystals) abundances versus ϕ [e.g., *Walker*, 1971] the variations of particle shape and density with ϕ ($d \ln (S)/d\phi$ and $d \ln (\rho)/d\phi$) are approximately constant and consistent with SFT, such that equation (C4) can be written as

$$\frac{dM}{d\phi} = K_3 l^6 \exp\left[-\frac{x}{\xi_0}\frac{l^{3(g+1)}}{g+1}\right] + K_s l^6 \exp\left[-\frac{x}{\xi_0}\frac{l^{3(g_s+1)}}{g_s+1}\right] + K_d l^6 \exp\left[-\frac{x}{\xi_0}\frac{l^{3(g_d+1)}}{g_d+1}\right] \tag{C5}$$

In this form where the effects of shape and density have their own normalization constants and SFT free parameters, K_s, K_d, g_s, and g_d, respectively, it is evident that the effects of variable particle shape and density produce a distribution that is the sum of three subpopulations, all of the SFT form.

NOTATION LIST

A, a, b constants in the log normal distribution;
A_r particle cross section area;
c constant in analytical size distributions;
e 2.71828;
$f(m' \rightarrow m)$ fragmentation function in the sequential fragmentation model;
g free parameter in the sequential transport model;
g_s free parameter for shape effects;
g_d free parameter for density effects;
k free parameter in Rosin-Rammler distribution;
K normalization constant for SFT model;
K_s normalization constant for shape effects;
K_d normalization constant for density effects;
l particle diameter;
M cumulative mass in a specified interval;
M_t total mass in a distribution;
m particle mass;
m' initial fragment mass prior to a sequential step of fragmentation;
$\bar{m}$ average mass per particle;
m_p mass of a particle at a distribution peak;
N cumulative number of particles in a specified interval;
$n(l)$ the number of particles of diameter l to $l + dl$;
$n(m)$ the number of particles of mass m to $m + dm$;
$n(x, m)$ the number of particles occurring at distance interval x to $x + dx$ and of mass m to $m + dm$;
P particle perimeter;
$p(\xi)$ the probability of a particle carried from location x' will be deposited at location x, used in sequential transport model;
S particle shape factor;
x location coordinate of sequential transport model;
x' initial location of a particle prior to a sequential step of transport;
α fine fraction exponent in generalized analytical distribution;
β coarse fraction exponent in generalized analytical distribution;
γ free parameter in the sequential fragmentation model;
ξ transport range function in sequential fragmentation model;
l particle diameter, e.g., μm, mm, m;
$\Gamma(\varepsilon)$ complete gamma function;
$\Gamma(\varepsilon, z)$ complementary, incomplete gamma function;
$\Upsilon(\varepsilon, z)$ incomplete gamma function;
ϕ nondimensional particle diameter;
σ size related to average particle size in Rosin-Rammler equation;
σ_ϕ standard deviation in phi units;
μ mass related to average mass in equations (14) and (15);
ν free parameter distribution of equations (14) and (15); for cases ν is set to 1/2 the distribution has been called the "Mott plot."

Acknowledgments. This work done under the auspices of the U.S. Department of Energy with support through Institutional Supporting Research and Development at Los Alamos National Laboratory. We thank Robert Ehrlich and Jack Horkowitz for CABFAC and QMODEL analysis of our data. Mathematicians at Los Alamos National Laboratory have given our mathematical derivation a helpful review.

REFERENCES

Anderson, R. S., and B. Hallet, Sediment transport by wind: Toward a general model, *Geol. Soc. Am. Bull.*, *97*, 523–535, 1986.
Bagnold, R. A., *The Physics of Blown Sand and Desert Dunes*, 265 pp., Methuen, London, 1941.
Bennett, J. G., Broken coal, *J. Inst. Fuel*, *10*, 22–39, 1936.
Brown, W. K., Comparison of a theory of sequential fragmentation with the initial mass function of stars. *Astrophys. Space Sci.*, *122*, 287–298, 1986.
Brown, W. K., A theory of sequential fragmentation and its astronomical applications, *J. Astrophys. Astron.*, *10*, 89–112, 1989.
Brown, W. K., R. R. Karpp, and D. E. Grady, Fragmentation of the universe, *Astrophys. Space Sci.*, *94*, 401–412, 1983.
Carey, S. N., and H. Sigurdsson, The influence of particle aggregation on deposition of distal tephra from the May 18, 1980, eruption of Mount St. Helens volcano, *J. Geophys. Res.*, *87*, 7061–7072, 1982.
Carey, S. N., and R. S. J. Sparks, Quantitative models of the fallout and dispersal of tephra from volcanic eruption columns, *Bull. Volcanol.*, *48*, 109–126, 1986.
Cashman, K. V., Crystal size distributions in igneous and metamorphic rocks, Ph.D. thesis, Johns Hopkins Univ., Baltimore, Md., 1986.
Criswell, C. W., Chronology and pyroclastic stratigraphy of the May 18, 1980, eruption of Mount St. Helens, Washington, *J. Geophys. Res.*, *92*, 10,237–10,266, 1987.
Denlinger, R. P., A model for generation of ash clouds by pyroclastic flows, with applications to the 1980 eruptions at Mount St. Helens, Washington, *J. Geophys. Res.*, *92*, 10,284–10,298, 1987.
Drinker, P., The size-frequency and identification of certain phagocytosed dusts, *J. Ind. Hyg.*, *7*, 305–316, 1925.
Ehrlich, R., and W. E. Full, Sorting out geology—Unmixing mixtures, in *Abuse of Statistical Methods in the Earth Sciences*, edited by W. Size, pp. 1–19, Oxford University Press, New York, 1987.
Eichelberger, J. C., and D. B. Hayes, Magmatic model for the Mount St. Helens blast of May 18, 1980, *J. Geophys. Res.*, *87*, 7727–7738, 1982.
Elderton, W. P., and N. L. Johnson, *Systems of Frequency Curves*, 216 pp., Cambridge University Press, New York, 1969.
Folk, R. L., A review of grain-size parameters, *Sedimentology*, *6*, 73–93, 1966.
Folk, R. L., *Petrology of Sedimentary Rocks*, 182 pp., Hemphill, Austin, Tex., 1974.
Full, E. F., Ehrlich, R., and J. C. Bezdeck, FUZZY QMODEL—A new approach for linear unmixing, *Math. Geol.*, *14*, 259–270, 1982.
Geer, M. R., and H. F. Yancey, Expression and interpretation of the size composition of coal, *Trans. Am. Inst. Min. Metall. Pet. Eng.*, *130*, 250–269, 1938.
Glicken, H., Rockslide-debris avalanche of May 18, 1980, Mount St. Helens Volcano, Washington, Ph.D. dissertation, 303 pp., Univ. of Calif., Santa Barbara, 1986.
Heiken, G., and K. Wohletz, *Volcanic Ash*, 246 pp., University of California Press, Berkeley, 1985.
Iversen, J. D., and B. R. White, Saltation threshold on Earth, Mars and Venus, *Sedimentology*, *29*, 111–119, 1982.
Kittleman, L. R., Jr., Application of Rosin's distribution in size-frequency analysis of clastic rocks, *J. Sediment. Petrol.*, *34*, 483–502, 1964.
Klovan, J. E., and A. T. Miesch, EXTENDED CABFAC and QMODEL computer programs for Q-mode factor analysis of compositional data, *Comput. Geosci.*, *1*, 161–178, 1976.
Kranck, K., and T. G. Milligan, Origin of grain size spectra of suspension deposited sediment, *Geo Mar. Lett.*, *5*, 61–66, 1985.
Krumbein, W. C., Size frequency of sediments and the normal phi curve, *J. Sediment. Petrol.*, *8*, 89–90, 1938.

Krumbein, W. C., and F. W. Tisdel, Size distributions of source rocks of sediments, *Am. J. Sci.*, *238*, 296–305, 1940.

Loveland, R. P., and P. H. Trivelli, Mathematical methods of frequency analysis of size of particles, *J. Franklin Inst.*, *204*, 193–217, 1927*a*.

Loveland, R. P., and P. H. Trivelli, Mathematical methods of frequency analysis of size of particles, *J. Franklin Inst.*, *204*, 377–389, 1927*b*.

McAlister, D., The law of the geometric mean, *Proc. R. Soc. London, Ser. A*, *29*, 367–376, 1879.

Martin, G., C. E. Blyth, and H. Tongue, Researches on the theory of fine grinding, *Trans. Ceram. Soc.*, *23*, 61–109, 1923.

Mellor, J. W., Jackson's and Purdy's surface factors, *Trans. Ceram. Soc.*, *9*, 94, 1910.

Nakamura, Y., The 1988 eruption of Bandai volcano, Japan: Grain size distribution, paper presented at Workshop on Volcanic Blasts, Int. Assoc. of Volcanol. and Chem. of the Earth's Interior, Mt. St. Helens, Washington, August 13–17, 1984.

Pearson, K., Contributions to the mathematical theory of evolution, II, Skew variation in homogeneous materials, *Philos. Trans. R. Soc. London, Ser. A*, *186*, 343–414, 1895.

Rietz, H. L., Frequency distributions obtained by certain transformations of normally distributed variates, *Ann. Math.*, *23*, 292–300, 1922.

Roller, P. S., Law of size distribution and statistical description of particulate materials, *J. Franklin Inst.*, *223*, 609–633, 1937.

Roller, P. S., Statistical analysis of the size distribution of particulate materials, with special reference to bimodal and frequency distributions: Correlations of quartile with statistical values, *J. Phys. Chem.*, *45*, 241–281, 1941.

Rosin, P. O., The influence of particle size in processes of fuel technology, *J. Inst. Fuel*, *11*, 26–41, 1937.

Rosin, P., and E. Rammler, The laws governing the fineness of broken coal, *J. Inst. Fuel*, *7*, 29–36, 1933.

Rosin, P., and E. Rammler, Die Kornzusammensetzung des Mahlgutes im Lichte der Wahrscheinlichkeitslehre, *Killoid Z.*, *67*, 16–26, 1934.

Schultz, P. H., and D. E. Gault, Atmospheric effects on Martian ejecta emplacement, *J. Geophys. Res.*, *84*, 7669–7687, 1979.

Sheridan, M. F., The mineralogy and petrology of the Bishop Tuff, Ph.D. dissertation, 165 pp., Stanford Univ., Stanford, Calif., 1965.

Sheridan, M. F., Particle-size characteristics of pyroclastic tuffs, *J. Geophys. Res.*, *76*, 5627–5634, 1971.

Sheridan, M. F., Emplacement of pyroclastic flows: A review, *Spec. Pap. Geol. Soc. Am.*, *180*, 125–136, 1979.

Sheridan, M. F., and R. G. Updike, Sugarloaf Mountain tephra—A Pleistocene rhyolitic deposit of base-surge origin in northern Arizona, *Geol. Soc. Am. Bull.*, *86*, 571–581, 1975.

Sheridan, M. F., K. H. Wohletz, and J. Dehn, Discrimination of grain-size subpopulations in pyroclastic deposits, *Geology*, *15*, 367–370, 1987.

Sigurdsson, H., S. Carey, W. Cornell, and T. Pescatore, The eruption of Vesuvius in A.D. 79, *Natl. Geogr. Res.*, *1*(3), 332–387, 1985.

Sparks, R. S. J., The dynamics of bubble formation and growth in magmas: A review and analysis, *J. Volcanol. Geotherm. Res.*, *3*, 1–37, 1978.

Sparks, R. S. J., and S. Brazier, New evidence for degassing processes during explosive volcanism, *Nature*, *295*, 218–220, 1982.

Theimer, O., Uber die "statistische mechanik" von zermahlungsvorgangen, *Kolloid Z.*, *128*, 1–16, 1952.

Turcotte, D. L., Fractals and fragmentation, *J. Geophys. Res.*, *91*, 1921–1926, 1986.

Vieweg, H. F., Particle-size distribution in some ground ceramic raw materials, *J. Am. Ceram. Soc.*, *18*, 25–29, 1935.

Walker, G. P. L., Grain-size characteristics of pyroclastic deposits, *J. Geol.*, *79*, 696–714, 1971.

Weibull, W., A statistical distribution function of wide applicability, *J. Appl. Mech.*, *18*, 293–297, 1951.

Wentworth, C. K., A scale of grade and class terms for clastic sediments, *J. Geol.*, *30*, 377–392, 1922.

White, B. R., Soil transport by winds on Mars, *J. Geophys. Res.*, *84*, 4643–4651, 1979.

White, B. R., and J. C. Schulz, Magnus effect in saltation, *J. Fluid Mech.*, *81*, 497–512, 1977.

Whitham, A. G., and R. S. J. Sparks, Pumice, *Bull. Volcanol.*, *48*, 209–223, 1986.

Wilson, L., Explosive volcanic eruptions, II, The atmospheric trajectories of pyroclasts, *Geophys. J. R. Astron. Soc.*, *30*, 381–392, 1972.

Wohletz, K. H., Mechanisms of hydrovolcanic pyroclast formation: Grain-size, scanning electron microscopy, and experimental studies, *J. Volcanol. Geotherm. Res.*, *17*, 31–64, 1983.

Wohletz, K. H., Explosive magma-water interactions: Thermodynamics, explosion mechanisms, and field studies, *Bull. Volcanol.*, *48*, 245–264, 1986.

Wohletz, K. H., and M. F. Sheridan, A model of pyroclastic surge, *Spec. Pap. Geol. Soc. Am.*, *180*, 177–193, 1979.

W. K. Brown, Math/Science Division, Lassen College, Susanville, CA 96130.

M. F. Sheridan, Department of Geology, Arizona State University, Tempe, AZ 85287.

K. H. Wohletz, Earth and Space Science Division, Los Alamos National Laboratory, Los Alamos, NM 87545.

(Received August 29, 1988;
revised February 13, 1989;
accepted June 7, 1989.)